energies

MDPI

Article

Numerical Study on the Combustion Properties of Ammonia/DME and Ammonia/DMM Mixtures

Yuanpu Zhang [1], Qian Wang [2], Liming Dai [2,*], Ming Zhang [1] and Chunkan Yu [3,*]

[1] Institute for Energy Research, Jiangsu University, Zhenjiang 212013, China
[2] School of Energy and Power Engineering, Jiangsu University, Zhenjiang 212013, China
[3] Institute of Technical Thermodynamics, Karlsruhe Institute of Technology, Engelbert-Arnold-Str. 4, 76131 Karlsruhe, Germany
* Correspondence: liming_dai@ujs.edu.cn (L.D.); chunkan.yu@kit.edu (C.Y.)

Abstract: Ammonia (NH_3) is considered a promising zero-carbon fuel and was extensively studied recently. Mixing high-reactivity oxygenated fuels such as dimethyl ether (DME) or dimethoxymethane (DMM) with ammonia is a realistic approach to overcome the low reactivity of NH_3. To study the combustion characteristics of NH_3/DMM and NH_3/DME mixtures, we constructed a NH_3/DMM chemical mechanism and tested its accuracy using measured laminar burning velocity (LBV) and ignition delay time (IDT) of both NH_3/DMM and NH_3/DME mixtures from the literature. The kinetic analysis of NH_3/DMM flames using this mechanism reveals that the CH_3 radicals generated from the oxidation of DMM substantially affects the oxidation pathway of NH_3 at an early stage of flame propagation. We investigated the formation of nitrogen oxides (NO_x) in NH_3/DMM and NH_3/DME flames and little difference can be found in the NO_x emissions. Using NH_3/DMM flames as an example, the peak NO_x emissions are located at an equivalence ratio (φ) of 0.9 and a DMM fraction of 40% in the conditions studied. Kinetic analysis shows that NO_x emission is dominated by NO, which primarily comes from fuel nitrogen of NH_3. The addition of DMM at 40% significantly promotes the reactive radical pool (e.g., H, O, and OH) while the maintaining a high concentration of NO precursors (e.g., HNO, NO_2, and N_2O), which results in a high reaction rate of NO formation reaction and subsequently generates the highest NO emissions.

Keywords: ammonia; dimethyl ether; dimethoxymethane; combustion mechanism; NO_x emission

Citation: Zhang, Y.; Wang, Q.; Dai, L.; Zhang, M.; Yu, C. Numerical Study on the Combustion Properties of Ammonia/DME and Ammonia/DMM Mixtures. *Energies* **2023**, *16*, 6929. https://doi.org/10.3390/en16196929

Academic Editors: Albert Ratner and Marco Marengo

Received: 24 August 2023
Revised: 25 September 2023
Accepted: 28 September 2023
Published: 2 October 2023

1. Introduction

Amidst the persisting global energy crisis and escalating concerns regarding environmental pollution, ammonia (NH_3) received significant attention as a zero-carbon fuel [1,2]. In the 1960s, extensive research was conducted in the United States to explore the feasibility of NH_3 combustion in military equipment such as gas turbines, compression ignition engines, and spark ignition engines [3,4]. However, these studies indicated that the direct utilization of NH_3 in combustion systems is challenging compared to conventional hydrocarbon fuels, such as low heating value, slow combustion rate, high ignition energy, and narrow flammable range. Therefore, it seems inevitable to modify or redesign traditional combustion systems to utilize pure NH_3 reliably to expand the operating range and improve the performance of pure NH_3 burners [3,4]. However, development of an existing combustion system can be costly. Hence, ongoing research is primarily directed towards preserving the integrity of present combustion equipment while harnessing the potential of NH_3 in conjunction with other highly reactive fuels. The incorporation of blended fuels serves as a booster to initiate or enhance the stable combustion of NH_3. In practical investigations concerning the blending of NH_3 with diverse fuels, a comprehensive analysis of the fuel combustion process is of utmost importance. It becomes imperative to comprehend the combustion properties via chemical kinetics to effectively enhance combustion stabilities, fuel efficiency, and curtail the emission of NO_x.

Different hydrocarbon fuels, such as hydrogen (H_2) [5,6], alkanes [7,8], and alcohols [9,10] were tested as combustion enhancer for NH_3. For instance, Wang et al. [5] measured the LBVs of NH_3/H_2 mixtures (0, 10, and 20% vol. H_2) at pressures from 1 to 5 bar, temperature from 360 K, and φ from 0.7 to 1.4 in a constant volume chamber and validated the accuracy of mechanisms developed by Okafor et al. [11], Mei et al. [12], and Shrestha et al. [13]. Dai et al. [6] proposed a combustion model for NH_3/H_2 blends by optimizing the mechanism of Glarborg et al. [14], which shows better performance than the mechanisms from Klippenstein et al. [15], Mathieu et al. [16], and Shrestha et al. [17] based on the IDTs measured (0–10% vol. H_2) at conditions (φ = 0.5, 1.0), pressures (20–75 bar), and temperatures (1040–1210 K) in a rapid compression machine. Wang et al. [18] coupled the skeletal n-heptane mechanism of Chang et al. [19] with the detailed NH_3/n-heptane mechanism of Dong et al. [20] to obtain an NH_3/n-heptane that can predict the IDTs of a NH_3/n-heptane mixture very well. Wang et al. [9] measured the LBVs of a NH_3/methanol (20–100% vol.) and NH_3/ethanol (20–100% vol. ethanol) mixture at 1 atm, temperatures from 298 to 448 K, and φ from 0.7 to 1.8 using the heat flux method and developed a NH_3/ethanol mechanism consisting of 91 species and 444 reactions.

In recent years, artificially synthesized polyoxymethylene dimethyl ethers (CH_3O-$(CH_2O)_n$-CH_3, $PODE_n$) attracted attention in that it can be used as fuel directly or as a fuel additive due to its high reactivity and low soot emission [21,22]. As a result, $PODE_n$ has great potential to be used as a promoter for NH_3 combustion in internal combustion engines. DME, as the simplest $PODE_n$, was investigated as a NH_3 combustion enhancer. Experimental results of the LBVs [23,24] and IDTs [25,26] of NH_3/DME mixtures indicate that DME performs well in enhancing the reactivity of NH_3. Xiao et al. [24] coupled the DME mechanism of Zhao et al. [27] with the NH_3 mechanism of Han et al. [28] and incorporated C–N interaction reactions from Shrestha et al. [29], Dai et al. [25], Konnov et al. [30], and others to develop an NH_3/DME mixed fuel mechanism consisting of 102 species and 594 reactions. Validation based on experimental data and literature confirms that the mechanism proposed by Xiao et al. [24], compared to the mechanisms of Dai et al. [25] and Issayev et al. [26], is not only more simplified, but also more accurate in predicting LBV and IDT. Meng et al. [31] focused on the variation in NO_x emissions during NH_3/DME combustion. They simulated the post combustion NO_x emissions of NH_3/DME using a detailed mechanism consisting of 221 species and 1597 reactions. The results show that the NO_x emissions did not decrease, but increase after DME was blended with NH_3. This phenomenon was also observed in the experiments of Gross et al. [32] on direct injection NH_3/DME compression ignition engines. Meng et al. [31] inferred that the generation of NO_x might be influenced by highly reactive radicals. Recently, Elbaz et al. [33] conducted further research on the blended combustion of DMM with NH_3. They measured the LBVs and Markstein length of NH_3/DMM using spherical freely propagating flames and developed a NH_3/DMM combustion mechanism by coupling the nitromethane mechanism of Shrestha et al. [34] and the DMM mechanism of Sun et al. [35], whereas the mechanism underestimates the measured LBVs for matures containing 20–60% DMM at lean conditions.

At present, there is no mechanism currently available that can simultaneously predict the combustion characteristics of NH_3/DME and NH_3/DMM. An accurate NH_3/DMM mechanism is vital to develop a combustion mechanism of NH_3 with heavier $PODE_n$. In this study, we developed a combustion mechanism for NH_3/DMM based on the work of Xiao et al. [24] and Li et al. [36]. The accuracy of the mechanism was validated using experimental data of NH_3/DMM [17,33] and NH_3/DME mixtures [24,25] from literature. We performed reaction path analysis, sensitivity analysis, and NO_x formation analysis of NH_3/DME and NH_3/DMM based on the present mechanism. Compared to previous studies [24,31,33], we presented a more comprehensive reaction pathway and provided further explanation for the peculiar phenomenon of NO_x emissions observed at different DMM fractions.

2. Kinetic Modeling

2.1. Numerical Approach

This study employs the one-dimensional (1D) free flame model and zero-dimensional (0D) ideal gas reactor model from Cantera [37] for the calculation of LBV and IDT.

The zero-dimensional (0D) ideal gas reactor model makes it so that the mixture behaves as an ideal gas. It means that the pressure, volume, and temperature of the mixture are related by the ideal gas law. The following is the governing equation for the zero-dimensional (0D) ideal gas reactor model:

$$\frac{d(\rho V)}{dt} = 0 \tag{1}$$

$$\rho V c_v \frac{dT}{dt} = -P\frac{dV}{dt} + \dot{q} - \sum \dot{m}_k h_k \tag{2}$$

$$\rho V c_v \frac{dY_k}{dt} = \dot{\omega}_k V \tag{3}$$

$$P = \rho RT \tag{4}$$

where ρ is the density, V is the reactor volume, c_v is the specific heat capacity at constant volume, T is temperature, P is pressure, $\dot{q}$ represents heat sources or losses, $\dot{m}_k$ is the mass flow rate of each species, and h_k is the enthalpy of species k, Y_k is the mole fraction of species k, $\dot{\omega}_k$ is the molar production rate of species k, and R is the gas constant.

The one-dimensional (1D) free flame model is stabilized in an axisymmetric stagnation flow and computes the solution along the stagnation streamline, using a similarity solution to reduce the three-dimensional governing equations to a single dimension. The following is the governing equation for the one-dimensional (1D) free flame model:

$$\frac{\partial \rho u}{\partial z} + 2\rho v = 0 \tag{5}$$

$$\rho u \frac{\partial v}{\partial z} + \rho V^2 = -\Lambda + \frac{\partial}{\partial z}\left(\mu \frac{\partial v}{\partial z}\right) \tag{6}$$

$$\rho c_p u \frac{\partial T}{\partial z} = \frac{\partial}{\partial z}\left(\lambda \frac{\partial T}{\partial z}\right) - \sum j_k \frac{\partial h_k}{\partial z} - \sum h_k W_k \dot{\omega}_k \tag{7}$$

$$\rho u \frac{dY_k}{dz} = -\frac{\partial j_k}{\partial z} + W_k \dot{\omega}_k \tag{8}$$

where ρ is the density, u is the axial velocity, v is the scaled radial velocity, Λ is the pressure eigenvalue (independent of z), μ is the dynamic viscosity, c_p is the heat capacity at constant pressure, T is the temperature, λ is the thermal conductivity, Y_k is the mass fraction of species k, j_k is the diffusive mass flux of species k, h_k is the enthalpy of species k, W_k is the molecular weight of species k, and $\dot{\omega}_k$ is the molar production rate of species k.

To ensure the post flame reaches equilibrium, the computational domain was set as a uniform spatial grid of 10 cm width. Additional points were automatically added in regions with steep gradients based on predefined ratios, slopes, and curves [38].

Sensitivity analysis of the LBV for NH_3/DME/air and NH_3/DMM/air mixtures was performed using a 'Brute force' method:

$$S_i = \frac{k_i}{S_l} \times \frac{\partial S_l}{\partial k_i} \tag{9}$$

where k_i represents the rate constant of the i-th reaction (1/s), and S_l is the LBV (cm/s). By varying k_i and calculating the resulting changes in S_l, normalized sensitivity coefficients S_i can be obtained. Each rate constant is increased by a factor of 2 by doubling the preexponential A factor while keeping those of the other reactions constant. A positive sensitivity coefficient indicates that the reaction promotes the flame propagation, while a negative

coefficient indicates that the reaction inhibits the flame propagation. An element flux analysis was performed to study the reaction path of the fuels under the experimental conditions. Rate of production (ROP) analysis was also performed to assist the interpretation of the results.

2.2. Mechanism Optimization

The mechanisms developed in this study are mainly drawn from Xiao et al. [24] and Li et al. [36], which serve as NH_3/DME and DMM submechanisms, respectively. The mechanism of Xiao et al. [31] coupled the DME mechanism of Zhao et al. [27] with the NH_3 mechanism of Han et al. [28] and incorporated C–N interaction reactions from Shrestha et al. [29], Dai et al. [25], and Konnov et al. [30]. The mechanism of Xiao et al. [24] performs well in predicting the LBVs [24] and IDTs [23] of NH_3/DME mixtures. The mechanism of Li et al. [36] based on the hieratical structure of 'reaction classes' was originally proposed by Curran et al. [39]. Validation based on experimental data and literature confirms that the mechanism proposed by Shrestha et al. [29] and Li et al. [36] is not only more simplified, but also more accurate in predicting LBVs and IDTs of DMM/air mixtures. We propose a new NH_3/DMM mechanism by coupling the NH_3/DME submechanism from Xiao et al. [24] and the DMM submechanism from Li et al. [36] and updating the reaction rates of some key reactions. The specific updates of the reaction rates are outlined in Table 1.

Table 1. Updates in the present mechanism. Units are s, mol, cm, and cal in $k = AT^n \exp\left(-\frac{E_a}{RT}\right)$.

No.	Reaction	A	n	Ea	Ref.
1	NH + NO = N_2O + H	2.7×10^{15}	−0.78	20.0	[40]
2	NH_2 + OH = NH + H_2O	2.04×10^{4}	2.52	−616.032	[41]
3	NH_3 + OH = NH_2 + H_2O	3.25×10^{12}	0.0	2120.0	[42]
4	NNH + O = NH + NO	5.2×10^{11}	0.388	−409.0	[15]
5	NH_2 + NO = H_2O + N_2	9.5×10^{16}	−1.44	268.0	[25]
6	NH_2 + NO_2 = H_2NO + NO	2.0×10^{19}	−2.369	870.0	[14]
7	HNO + O_2 = NO + HO_2	2.0×10^{13}	0.0	14896.0	[25]
8	H_2NO + NO_2 = HONO + HNO	6.0×10^{12}	0.0	2000.0	[25]
9	N_2H_3 + HO_2 = N_2H_4 + O_2	9.2×10^{5}	1.94	2126.1	[25]
10	H + O_2 + M = HO_2 + M	4.65×10^{12}	0.44	0.0	[43]
11	H + OH + M = H_2O + M	3.5×10^{22}	−2.0	0.0	[44]
12	O + H_2O = OH + OH	6.7×10^{7}	1.704	14986.8	[45]
13	HO_2 + OH = H_2O + O_2	1.93×10^{20}	−2.49	584	[46]
14	HO_2 + O = O_2 + OH	1.0×10^{13}	0.0	−4452	[47]
15	CH_2 + O_2 = HCO + OH	1.06×10^{13}	0.0	1500.0	[44]
16	HCO + O_2 = CO + HO_2	13.45×10^{12}	0.0	400.0	[44]
17	CO + OH = CO_2 + H	8.7×10^{4}	2.053	−355.7	[48]
18	$CH_3OCH_2OCH_3$ + H = $CH_3OCH_2OCH_2$ + H_2	5.04×10^{6}	2.3	6453.155	[49]
19	$CH_3OCH_2OCH_3$ + H = $CH_3OCHOCH_3$ + H_2	2.18×10^{10}	1.155	6548.757	[49]
20	$CH_3OCH_2OCH_3$ + M = CH_3OCH_2O + CH_3 + M	2.33×10^{19}	−0.66	84139.5	[50]
21	$CH_3OCH_2OCH_3$ + NH_2 = $CH_3OCH_2OCH_2$ + NH_3	1.8×10^{0}	3.61	4353.0	est DME
22	$CH_3OCH_2OCH_3$ + NH_2 = $CH_3OCHOCH_3$ + NH_3	3.79×10^{3}	2.426	4475.0	est DME
23	$CH_3OCH_2OCH_3$ + NO_2 = $CH_3OCH_2OCH_2$ + HONO	5.8×10^{1}	3.5	23755.0	est DME
24	$CH_3OCH_2OCH_3$ + NO_2 = $CH_3OCHOCH_3$ + HONO	9.93×10^{2}	3.112	22010.0	est DME
25	$CH_3OCH_2OCH_3$ + NO_2 = $CH_3OCH_2OCH_2$ + HNO_2	6.5×10^{2}	3.0	23176.0	est DME
26	$CH_3OCH_2OCH_3$ + NO_2 = $CH_3OCHOCH_3$ + HNO_2	1.11×10^{4}	2.667	21473.0	est DME

The updated reaction rate constants for R1, R2, R3, and R4 are referenced from the literature [15,40–42]. By modifying the reaction rate constant of R1, R2, R3, and R4, the accuracy of the mechanism is improved while adjusting the contribution of different elementary reaction pathways in the combustion process of ammonia.

$$NH + NO = N_2O + H \quad (R1)$$

$$NH_2 + OH = NH + H_2O \quad (R2)$$

$$NH_3 + OH = NH_2 + H_2O \quad (R3)$$

$$NNH + O = NH + NO \quad (R4)$$

The reaction rate constants for reactions R5 and R6 were adjusted based on the literature [14,25]. Additionally, reactions R7, R8, and R9 were introduced to further optimize the reaction pathway of NH_3 during the initial stages of combustion. These adjustments effectively enhanced the accuracy of the mechanism's predictions for NH_3 IDT.

$$NH_2 + NO = H_2O + N_2 \quad (R5)$$

$$NH_2 + NO_2 = H_2NO + NO \quad (R6)$$

$$HNO + O_2 = NO + HO_2 \quad (R7)$$

$$H_2NO + NO_2 = HONO + HNO \quad (R8)$$

$$N_2H_3 + HO_2 = N_2H_4 + O_2 \quad (R9)$$

Reactions R10 and R11 are important pathways for the consumption of H radical and play a suppressive role in the combustion of NH_3/DMM/air and NH_3/DME/air mixtures. In this study, the reaction rate of R10 decreased at low temperatures and increased at high temperatures based on data from Fernandes et al. [43]. The reaction rate of R11 was slightly decreased based on data from GRI 3.0 [44].

$$H + O_2 + M = HO_2 + M \quad (R10)$$

$$H + OH + M = H_2O + M \quad (R11)$$

Under lean conditions with a high fraction of NH_3, O radicals tend to react with H_2 and H_2O, while under rich conditions, O radicals tend to react with H_2 and CH_3, both of which play important promoting roles in NH_3/DMM/air and NH_3/DME/air mixtures. In this study, the reaction rate of R12 is increased based on data from Sutherland et al. [45].

$$O + H_2O = OH + OH \quad (R12)$$

Under conditions with a low fraction of NH_3, reactions R13 and R14 suppress the combustion of NH_3/DMM/air and NH_3/DME/air mixtures by consuming radicals. In this study, the reaction rate of R13 is increased and that of R14 is decreased based on data from Burke et al. [46] and Baulch et al. [47], respectively, to adjust the consumption pathway of HO_2.

$$HO_2 + OH = H_2O + O_2 \quad (R13)$$

$$HO_2 + O = O_2 + OH \quad (R14)$$

Reactions R15, R16, and R17 are important pathways for CO_2 formation. The promoting effect of reaction R15 on the combustion of NH_3/DMM/air and NH_3/DME/air mixtures becomes more significant with an increase in the fraction of hydrocarbon fuels in the mixture, while reaction R16 starts to inhibit combustion as the fraction of hydrocarbon fuels decreases. Reaction R17 is an important reaction that consumes CO to produce CO_2, playing a promoting role in the combustion of NH_3/DMM/air and NH_3/DME/air mixtures. In this study, the reaction rates of R15 and R16 are updated based on data from GRI 3.0 [44], and the reaction rate of R17 is decreased based on data from Jshi et al. [48], improving the accuracy of the CO_2 generation pathway in the mechanism.

$$CH_2 + O_2 = HCO + OH \quad (R15)$$

$$HCO + O_2 = CO + HO_2 \quad \text{(R16)}$$

$$CO + OH = CO_2 + H \quad \text{(R17)}$$

Reactions R18, R19, and R20 are important components of the low-temperature oxidation mechanism of DMM. Reactions R18 and R19 inhibit the combustion of the NH_3/DMM/air mixture by consuming H radicals, while reaction R20 promotes the combustion of the mixture by generating CH_3OCH_2O and CH_3 radicals through the decomposition of DMM. The reaction rates of R18 and R19 are increased based on simulation data from Vermeire et al. [49], and reaction R20 is updated based on the molecular collision effects in the DMM decomposition process proposed by Jacobs et al. [50]. Through these updates to the aforementioned reactions, the low-temperature oxidation pathway of DMM in this mechanism is improved.

$$CH_3OCH_2OCH_3 + H = CH_3OCH_3OCH_2 + H_2 \quad \text{(R18)}$$

$$CH_3OCH_2OCH_3 + H = CH_3OCHOCH_3 + H_2 \quad \text{(R19)}$$

$$CH_3OCH_2OCH_3 + M = CH_3OCH_2O + CH_3 + M \quad \text{(R20)}$$

Furthermore, reactions R21–R26 are the interactions between DMM and nitrogen estimated based on the NH_3/DME/air mechanism proposed by Xiao et al. [24] in this study.

$$CH_3OCH_2OCH_3 + NH_2 = CH_3OCH_3OCH_2 + NH_3 \quad \text{(R21)}$$

$$CH_3OCH_2OCH_3 + NH_2 = CH_3OCHOCH_3 + NH_3 \quad \text{(R22)}$$

$$CH_3OCH_2OCH_3 + NO_2 = CH_3OCH_3OCH_2 + HONO \quad \text{(R23)}$$

$$CH_3OCH_2OCH_3 + NO_2 = CH_3OCHOCH_3 + HONO \quad \text{(R24)}$$

$$CH_3OCH_2OCH_3 + NO_2 = CH_3OCH_3OCH_2 + HNO_2 \quad \text{(R25)}$$

$$CH_3OCH_2OCH_3 + NO_2 = CH_3OCHOCH_3 + HNO_2 \quad \text{(R26)}$$

The complete mechanism is composed of 108 species and 615 reversible reactions.

3. Results and Discussion

3.1. Mechanism Validation

The present mechanism is validated against the measured LBVs of NH_3/DMM/air and NH_3/air mixtures from literature as shown in Figure 1. The calculated LBVs agree very well with the measured LBVs of NH_3/DMM/air mixtures at most conditions, only slight underestimation up to ~2 cm/s is observed for pure DMM/air mixtures. For NH_3/air mixtures, the calculated LBVs lies in the cross-section of the experimental data from literature. The validation of the present mechanism is also performed against the LBV of NH_3/DME/air mixtures under ambient condition as shown in Figure 2. The present mechanism predicts the LBVs precisely for NH_3/DME mixtures except that it slightly underestimates the LBVs of pure DME by 3cm/s from φ = 0.7 to 1.3. For NH_3 with 50% DME fraction at elevated temperature and pressures, the validation is firstly performed at T_u = 298 K and P_u ranges from 1 to 4 atm as shown in Figure 3a. The present mechanism generally predicts the LBVs well at most conditions, albeit the biggest underestimation up to 5 cm/s is observed at the leanest condition for P_u = 1 atm. The discrepancy mitigates at elevated pressures. The overall performance is further improved for all three pressures at elevated temperature T_u = 373 K as shown in Figure 3b.

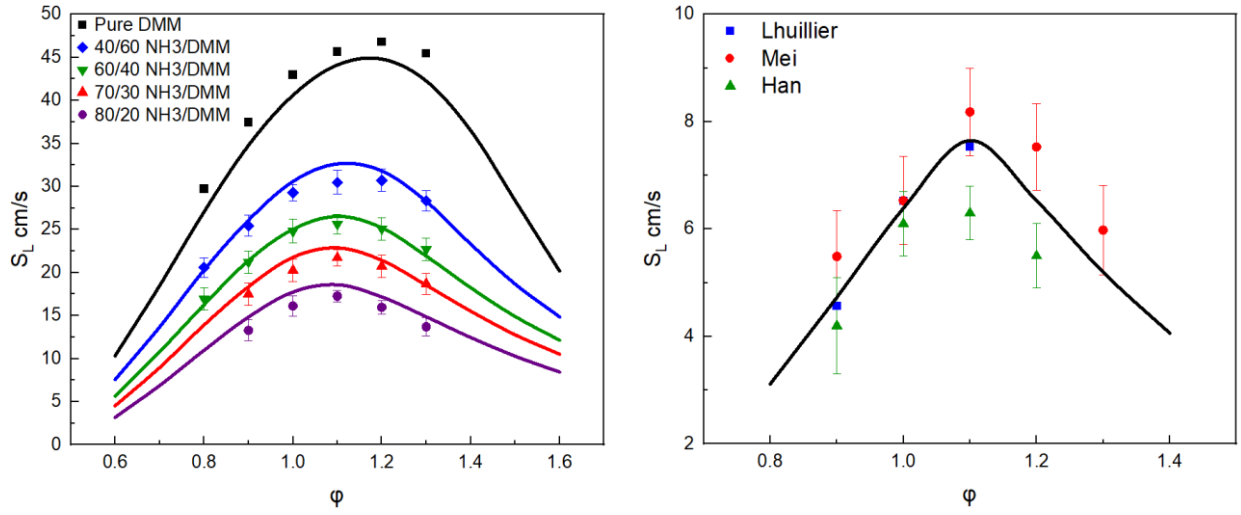

(**a**) NH_3/DMM/air (**b**) NH_3/air

Figure 1. Effect equivalence ratio on the LBVs of DMM/air, NH_3/DMM/air (**a**), and NH_3/air (**b**) mixtures at T_u = 298 K and P_u = 1 bar. The experimental data for the DMM/air mixture are obtained from Shrestha et al. [17], the NH_3/DMM/air mixture from Elbaz et al. [33], and the NH_3/air mixture from Lhuillier et al. [51], Mei et al. [12], and Han et al. [52]. The solid line represents the predicted results of the present mechanism.

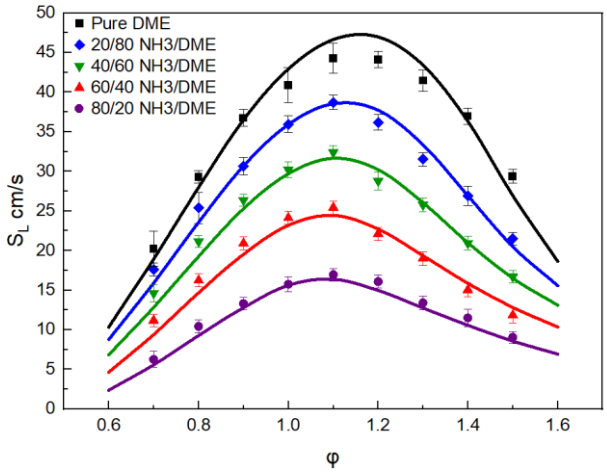

Figure 2. Effect of the equivalence ratio on the LBV of the NH_3/DME/air mixture at T_u = 298 K and P_u = 1 bar. The experimental data for DME/air and NH_3/DME/air mixtures are obtained from Xiao et al. [24]. The solid line represents the predicted results of the present mechanism.

Figure 4 illustrates the comparison of calculated IDTs using the present mechanism and the measured IDTs of the NH_3/DME mixture from Issayev et al. [26]. As can be seen, the present mechanism can accurately predict the measurements at all four conditions. Figures 5 and 6 illustrate the comparison between the predictions of the present mechanism and the measured IDTs of pure DME and pure NH_3 from Dai et al. [25]. As shown in the figure, the present mechanism accurately predicts IDTs of pure DME and pure NH_3. In general, the present mechanism can accurately predict the LBVs of NH_3/DMM/air and NH_3/DME/air mixtures and the IDTs of the NH_3/DME/air mixture as well. To our knowledge, there are no IDT measurements of NH_3/DMM available at present, and further validation against the IDTs of NH_3/DMM will be added in our future study. The present mechanism is employed to perform a chemical kinetic analysis of NH_3/DMM flames in the next section.

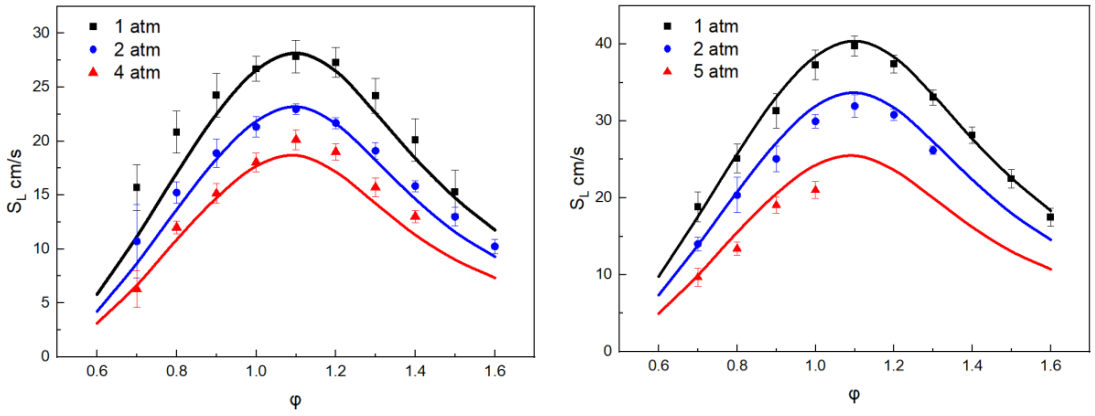

(**a**) T_u = 298 K (**b**) T_u = 373 K

Figure 3. Effect of the equivalence ratio on the LBV of the NH_3/DME/air mixture with X_{DME} = 50% at under different pressures, at 298 K (**a**) and 373 K (**b**). The experimental data for the NH_3/DME/air mixture are obtained from Yin et al. [23].

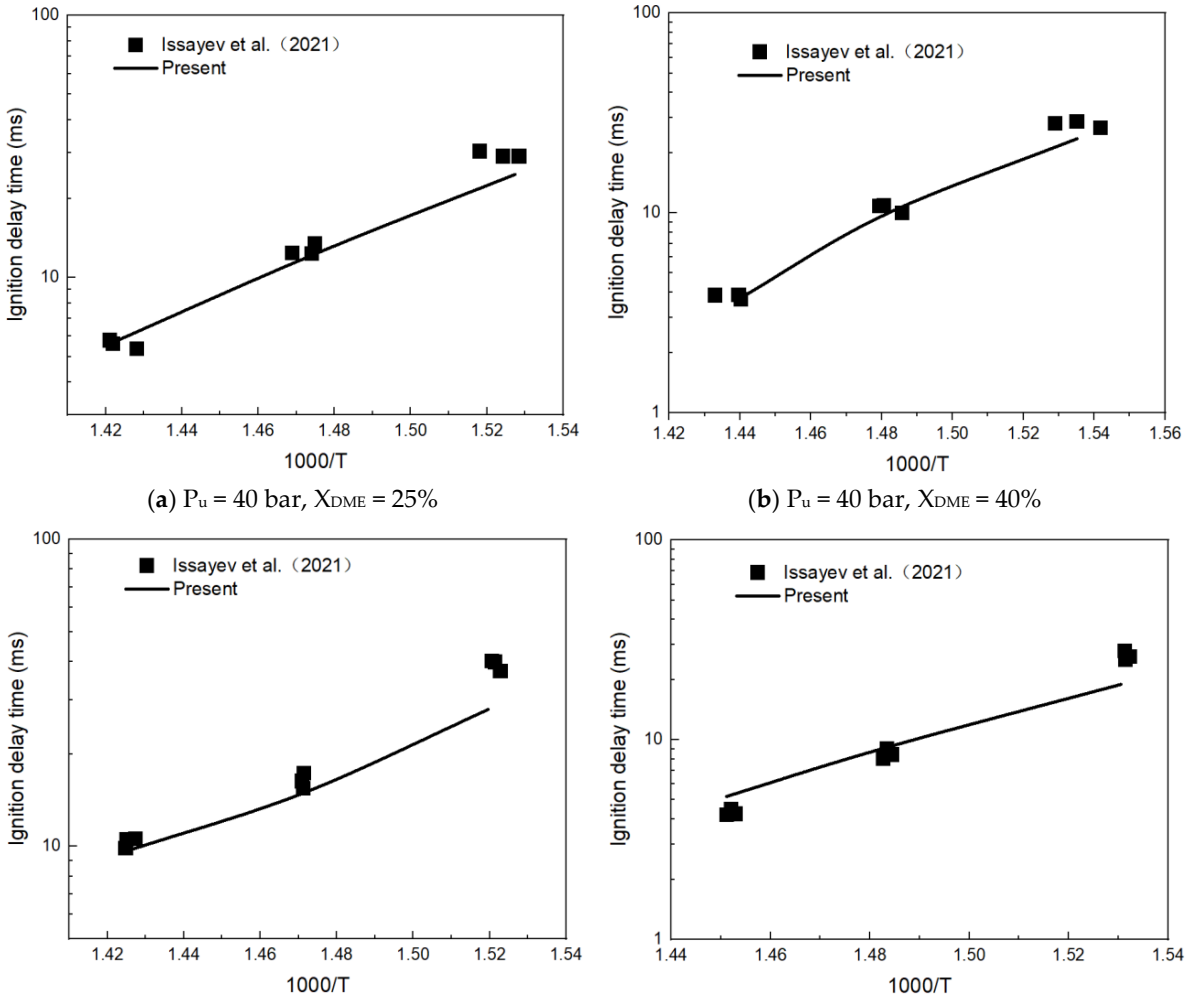

(**a**) P_u = 40 bar, X_{DME} = 25% (**b**) P_u = 40 bar, X_{DME} = 40%

(**c**) P_u = 20 bar, X_{DME} = 25% (**d**) P_u = 20 bar, X_{DME} = 40%

Figure 4. Effect of temperature on the IDT of the NH_3/DME/air mixture at φ = 1.0. The working conditions corresponding to (**a**–**d**) are: P_u = 40 bar/X_{DME} = 25%, P_u = 40 bar/X_{DME} = 40%, P_u = 20 bar/X_{DME} = 25%, P_u = 20 bar/X_{DME} = 40%. The experimental data for the IDT of the NH_3/DME/air mixture are obtained from Issayev et al. [26].

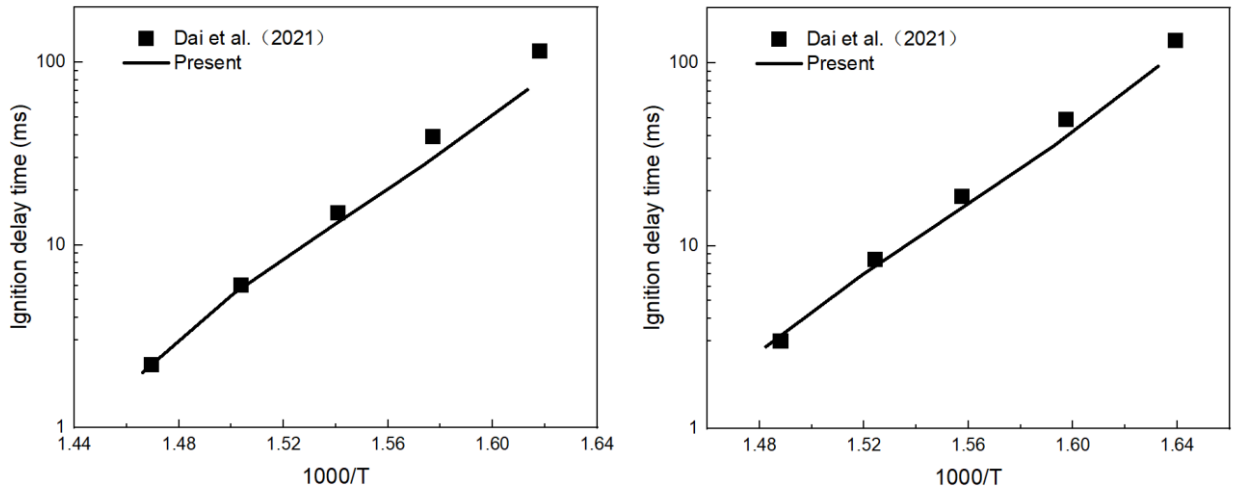

(**a**) P_u = 60 bar, φ = 0.5 (**b**) P_u = 60 bar, φ = 1.0

Figure 5. Effect of temperature on the IDT of the DME/air mixture at P_u = 60 bar/φ = 0.5 (**a**) and P_u = 60 bar/φ = 1.0 (**b**). The experimental data for the IDT of the DME/air mixture are obtained from Dai et al. [25].

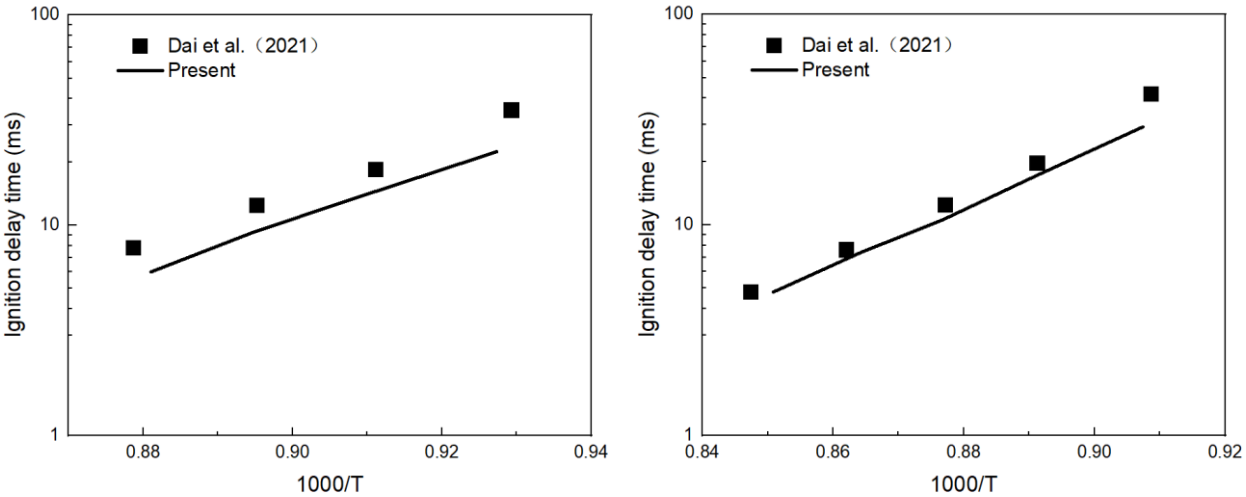

(**a**) P_u = 60 bar, φ = 0.5 (**b**) P_u = 60 bar, φ = 1.0

Figure 6. Effect of temperature on the IDT of the NH_3/air mixture at P_u = 60 bar/φ = 0.5 (**a**) and P_u = 60 bar/φ = 1.0 (**b**). The experimental data for the IDT of the NH_3/air mixture are obtained from Dai et al. [25].

3.2. Kinetic Analysis

3.2.1. Reaction Pathway and Sensitivity Analysis

To investigate the overall oxidation pathways of NH_3/DME/air mixtures, we conducted a reaction path analysis by tracing nitrogen (Figure 7a) and carbon (Figure 7b), respectively, at T_u = 298 K, P_u = 1 bar, φ of 0.9, and a DME substitution rate of 40%. Similar to the reaction path of pure ammonia [13,26], the first step for ammonia is dehydrogenation to form NH_2, followed by the generation of N_2 through four key intermediate species: NH, NHO, NNH, and NO. At a flame temperature of 1000 K, NO can be converted to NO_2, but its influence diminishes as the temperature increases. When the flame temperature reaches 2000 K, N_2O can be further converted to N_2. When DMM fraction reaches 40%, NH_2 reacts with CH_3 generated from the thermal decomposition of DMM to produce a significant amount of CH_3NH_2. At a flame temperature of 1500 K, the flux of the $NH_2 \rightarrow CH_3NH_2$ reaction pathway will exceed 60% in the N element reaction path.

This phenomenon was also observed in previous studies on NH_3/DME/air [23,24] and NH_3/CH_4/air [53] mixtures, indicating that the addition of DMM has a significant impact on the early oxidation process of NH_3. From the reaction pathway diagram of ammonia, it can be observed that at a flame temperature of 1500 K, NO is mainly generated through three pathways: 1.$NH_3 \rightarrow NH_2 \rightarrow NH \rightarrow NO$, 2.$NH_3 \rightarrow NH_2 \rightarrow HNO \rightarrow NO$, and 3.$NH_3 \rightarrow NH_2 \rightarrow NH \rightarrow NHO \rightarrow NO$. The fluxes of NO generated through these channels do not exceed 20%. However, as the fuel oxidation process progresses, the DMM component in the fuel is consumed first, and the temperature increases, leading to the oxidation of NH_3. Additionally, the accumulated CH_3NH_2 in the early stage will also be converted to NO. The high temperature will suppress the flux of the $NO \rightarrow N_2$ pathway, resulting in the accumulation of NO.

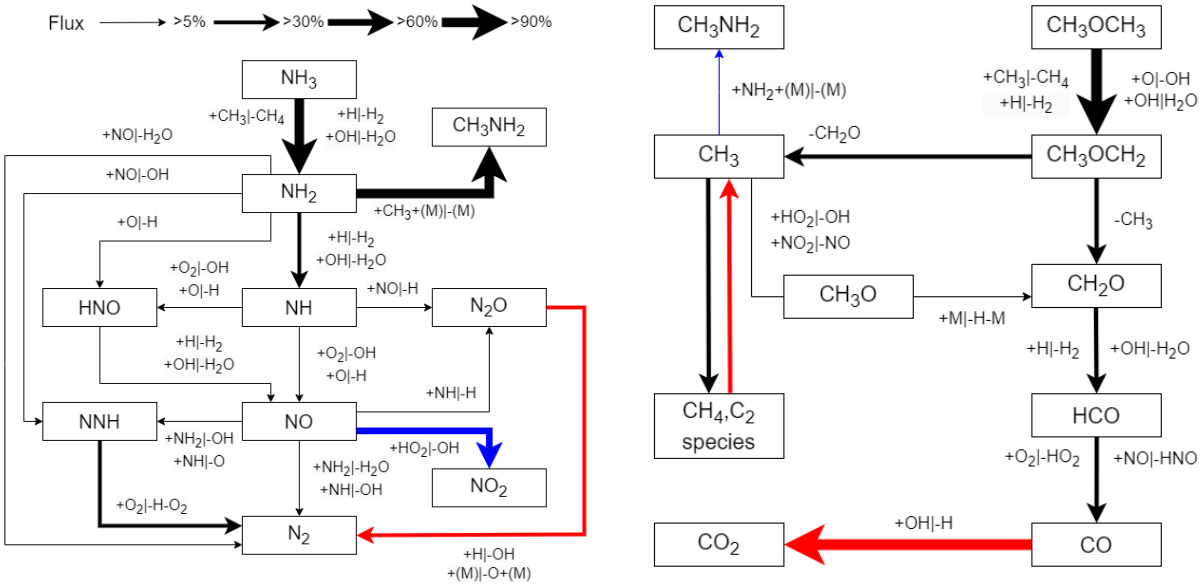

Figure 7. The reaction pathways for carbon (**a**) and nitrogen (**b**) under the conditions of T_u = 298 K and P_u = 1 bar, and φ = 0.9 and X_{DME} = 40%. The black line represents the reaction pathways at a flame temperature of 1500 K, while the blue and red lines represent the additional key component reaction pathways at flame temperatures of 1000 K and 2000 K, respectively.

As shown in Figures 7b and 8, the C–N interaction has a relatively small impact on the oxidation of DME and DMM. DME first reacts with H, OH, O, and CH_3 radicals to undergo dehydrogenation, forming CH_3OCH_2. The CH_3OCH_2 radical primarily undergoes thermal dissociation to produce CH_3 and CH_2O. At lower flame temperature (1000 K), a small amount of CH_3 reacts with NH_2 under the influence of C–N interaction, leading to the formation of CH_3NH_2. As the flame temperature increases to 1500 K, more than 60% of the CH_3 radicals undergo self-recombination and further oxidation to form C_2 species (e.g., C_2H_6 and C_2H_5) or reacts with H, HO_2, and CH_2O radicals to produce CH_4. Meanwhile, CH_2O is further oxidized to CO through the pathway $CH_2O \rightarrow HCO \rightarrow CO$. When the flame temperature reaches 2000 K, CH_4 and C_2 species are involved in oxidation reactions, and CO is gradually completely oxidized to CO_2 by OH radicals.

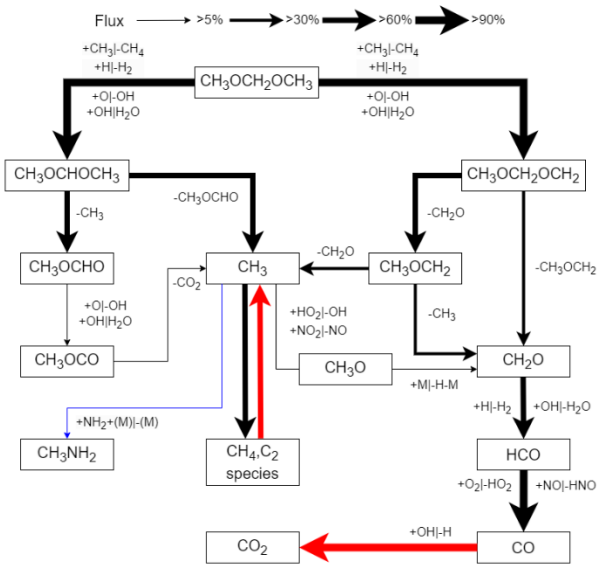

Figure 8. The reaction pathways of carbon at T_u = 298 K, P_u = 1 bar, φ = 0.9, and X_{DMM} = 40%. The black line represents the reaction pathways at a flame temperature of 1500 K, while the blue and red lines represent the additional key component reaction pathways at flame temperatures of 1000 K and 2000 K, respectively.

The sensitivity analysis of the LBV for pure NH_3, NH_3/DME, and NH_3/DMM mixtures are performed at T_u = 298 K, P_u = 1 bar, and φ of 0.9 as shown Figure 9. Consistent with the findings of Xiao et al. [24], the reactions involving H radicals, namely H + O_2 = O + OH and H + O_2 (+M) = HO_2 (+M), have the most significant promoting and inhibiting effects on the LBV of pure NH_3. Additionally, the reactions involving NH_2 radicals, NH_2 + NO = NNH + OH and NH_2 + NO = H_2O + N_2, correspond to two reaction pathways ($NH_2 \rightarrow NNH \rightarrow N_2$ and $NH_2 \rightarrow N_2$) for the oxidation of NH_2 as shown in Figure 7. Furthermore, the reactions NH_3 + O = NH_2 + OH and HO_2 + NH_2 = NH_3 + O_2 are also important in the $NH_3 \rightarrow NH_2$ reaction pathway. Overall, the concentration variations of highly reactive radicals such as H and key intermediate species such as NH_2 play a crucial role in the combustion process of pure ammonia. Figure 9b represents the sensitivity analysis of the LBVs for NH_3/DME/air and NH_3/DMM/air mixtures with 40% DMM or DME fraction at T_u = 298 K, P_u = 1 bar, and φ of 0.9. For both flames, the chain branching reaction H + O_2 = O + OH always exhibits the highest sensitivity. Other highly sensitive reactions, such as CO + OH = CO_2 + H and HCO + M = CO + H + M, are crucial for the reaction pathway $HCO \rightarrow CO \rightarrow CO_2$ (as shown in Figures 7 and 8) and achieving complete oxidation of carbon to CO_2. The reaction H + O_2 (+M) = HO_2 (+M) plays the most significant inhibitory role in the combustion of both flames, followed by the key reactions of NH_3 oxidation to NH_2 radicals: HO_2 + NH_2 = NH_3 + O_2 and NH_3 + OH = H_2O + NH_2. Furthermore, CH_3, as a key radical in the oxidation of DME and DMM, is involved in many important reactions that affect the LBV. For example, the reaction CH_3 + HO_2 = CH_3O + OH is crucial for driving the oxidation of CH_3 radicals. The reaction CH_3 + H (+M) = CH_4 (+M) is the main reaction causing the reduction in CH_3 radicals to CH_4 at lower flame temperatures and inhibiting the combustion process.

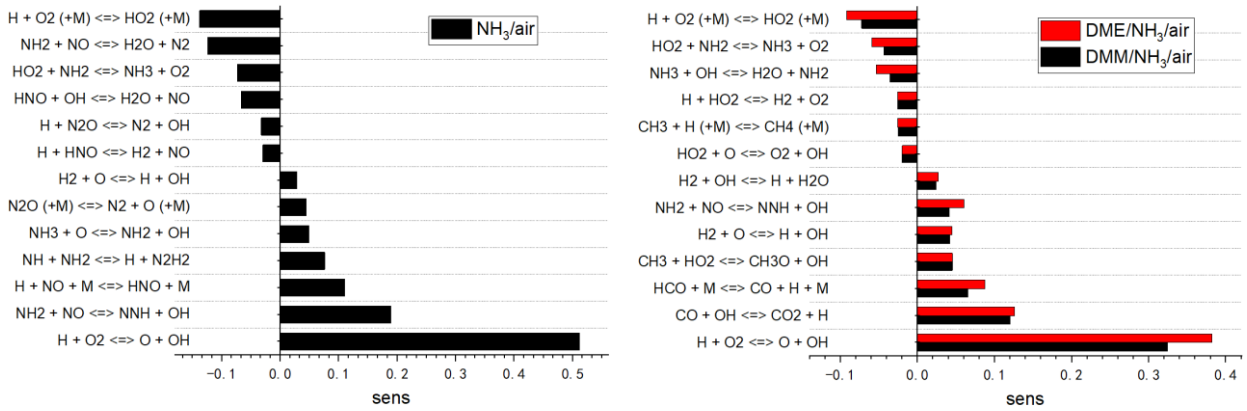

(**a**) NH_3/air (**b**) NH_3/DME/air and NH_3/DMM/air

Figure 9. Sensitivity analysis of the LBVs for NH_3/air (**a**), NH_3/DME/air, and NH_3/DMM/air (**b**) mixtures at T_u = 298 K, P_u = 1 bar, φ = 0.9, and XDME = XDMM = 40%.

Overall, the main reactions controlling the LBVs of NH_3/DME/air and NH_3/DMM/air mixtures are almost identical, the LBVs are primarily dominated by the reactions of small radicals, and no C–N interaction reactions or fuel dissociations were found among these reactions. This suggests that the variations in LBVs for both mixtures are primarily influenced by changes in the shared OH, H, and O radical pool during the oxidation of NH_3 and DME, rather than by mutual reactions between C and N elements. This finding is consistent with the research results of Xiao et al. [24] and Elbaz et al. [33].

3.2.2. NO_x Emission Analysis

The effect of DMM and DME addition on NO_x emissions and temperature as a function of φ is shown in Figure 10. For NH_3/DME/air mixtures with different DME fraction, a similar trend can be observed that the NO_x emission initially increases from leanest condition to φ = 0.9 and then decrease after the peak. The contribution of thermal NO_x from pure DME combustion is negligible compared to the fuel NO_x coming from NH_3 as shown in Figure 10a. This suggests that the NO_x emissions generated during laminar burning of NH_3/DME/air mixtures are influenced to some extent by temperature, but the relationship with temperature is not directly correlated. Notably, under different DME fractions, the temperature increases with higher DME fractions, while NO_x emissions exhibit an initial increase followed by a decrease, peaking within the range of 40% to 50%. As shown in Figure 10b, the trend of NO_x emissions for NH_3/DMM/air mixtures is similar to that of NH_3/DME/air mixtures, but the peak NO_x emissions occur at φ of 0.9 within the range of the 30% to 40% DMM fraction.

Kinetic analysis reveals that the main component of NO_x emissions in NH_3/DME/air and NH_3/DMM/air mixtures is NO, while the emissions of other nitrogen oxides are approximately two orders of magnitude lower than NO. This study conducted a rate of production analysis on NO at T_u = 298 K and P_u = 1 bar, with φ of 0.9 and DME (Figure 11a) and DMM (Figure 11b) fractions of 40%. As shown in Figure 11, the generation and consumption of NO in NH_3/DME and NH_3/DMM mixtures are primarily influenced by six reactions. The reactions involving H + NO_2 = NO + OH, H + HNO = H_2 + NO, HNO + OH = H_2O + NO, and H + NO = NH + O contribute to the production of NO, while the reactions HO_2 + NO = NO_2 + OH and NH + NO = H + N_2O participate in NO consumption. It is noteworthy that four reactions involve H radicals, and three reactions involve OH radicals, indicating the significant impact of highly reactive radicals such as H and OH on NO_x emissions.

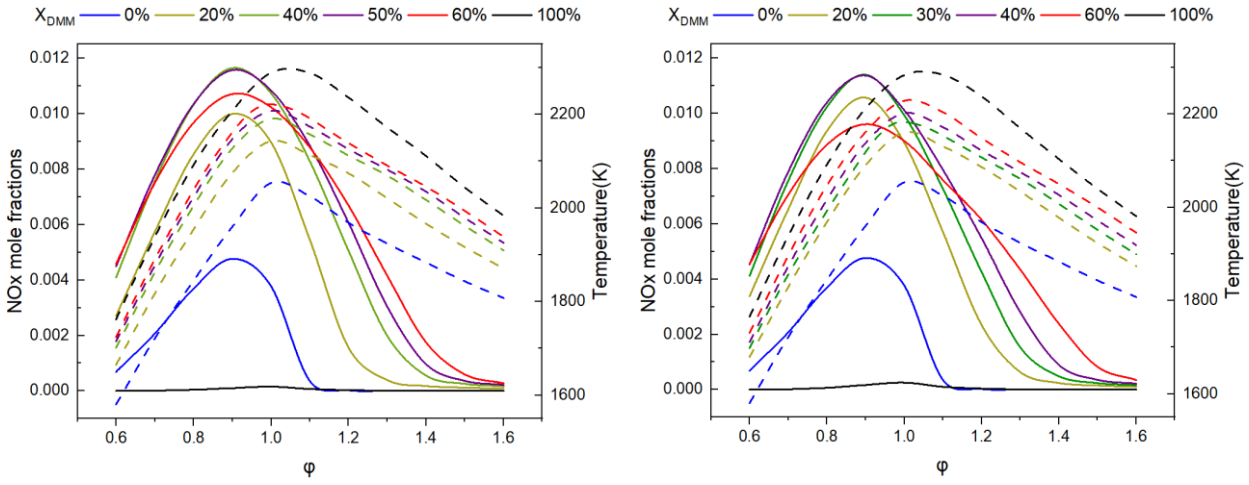

(**a**) NH_3/DME/air (**b**) NH_3/DMM/air

Figure 10. Effects of the equivalence ratio on NO_x emissions (solid lines) and adiabatic flame temperature (dashed lines) for the combustion of NH_3/DMM/air (**a**) and NH_3/DME/air (**b**) mixtures at T_u = 298 K and P_u = 1 bar.

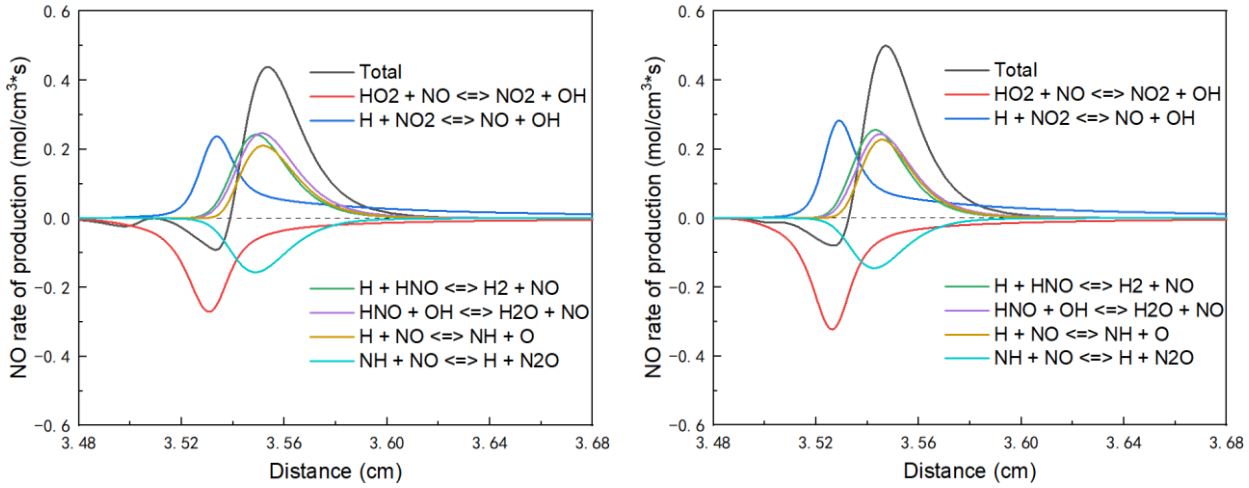

(**a**) NH_3/DME/air (**b**) NH_3/DMM/air

Figure 11. During the combustion of NH_3/DME/air (**a**) and NH_3/DMM/air (**b**) mixtures, the six reactions that have the greatest impact on the NO production rates under the conditions of T_u = 298 K, P_u = 1 bar, φ = 0.9, and $X_{DME} = X_{DMM}$ = 40%.

To investigate the impact of highly reactive free radicals such as H and OH on NO_x emissions, this study focuses on the analysis of the ROP and concentration changes of the H radical in NH_3/DMM/air mixtures as an example. As shown in Figure 12a, under different DMM fractions, all NO reactions involving the H radical exhibit a promoting effect on the NO formation. The ROP of these reactions demonstrates a similar trend to Figure 11, where the NO emissions are higher at X_{DMM} = 40% compared to X_{DMM} = 20% and X_{DMM} = 80%. Further analysis of the concentration changes of the H radical and related NO precursors (e.g., NO_2, HNO, and N_2O) at the same flame length is presented in Figure 12b. It is evident that both the H radical and NO precursors show a monotonic correlation with the DMM fraction, meaning that the concentration of the H radical increases overall while the concentration of NO precursors decreases with an increase in the DMM fraction. This is because the combustion process of DMM generates a significantly higher concentration of the H radical compared to NH_3, while the formation of NO precursors relies mainly on the oxidation of NH_3. In the NH_3/DMM/air combustion process, a lower DMM fraction

leads to a decrease in NO emissions due to the lack of highly reactive free radicals such as the H radical, while a higher DMM fraction results in a decrease in NO emissions due to the deficiency of NO precursors. Only within an appropriate range of the DMM fraction can the generation of an appropriate concentration of highly reactive free radicals such as the H radical and the presence of NO precursors lead to the peak generation of NO during the combustion process. Figure 13 compares the concentration changes of the H radical and NO precursors in NH_3/DME/air and NH_3/DMM/air mixtures at T_u = 298 K, P_u = 1 bar and φ = 0.9. This demonstrates that under the same conditions, the addition of DMM produces a higher concentration of the H radical compared to DME, while the concentration of NO precursors is lower than that of DME. This explains why the peak NO_x emissions in NH_3/DMM/air combustion with a blending ratio of hydrocarbon fuel are 10% lower than those of NH_3/DME/air. In conclusion, the fraction of DME or DMM in NH_3 combustion does not show the monotonical effect of NO_x emissions. One of the crucial factors influencing the phenomenon is the 'trade-off' relationship between highly reactive radicals (e.g., H, OH, and O) and NO precursors caused by DME or DMM addition.

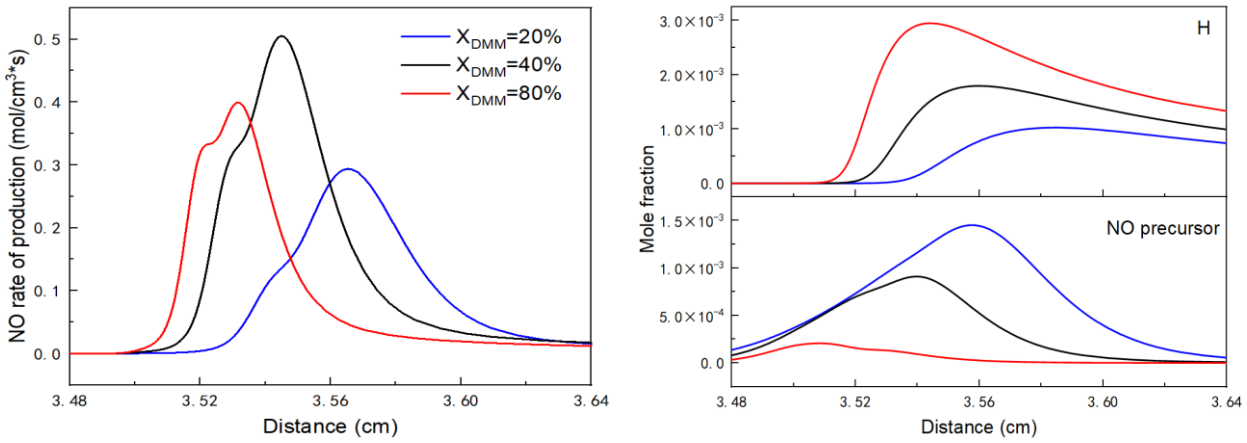

Figure 12. Effect of different DMM fractions on the production rates of NO involving the H radical (**a**) and the concentration variations of H radical and NO precursors associated with these reactions (**b**) under the conditions of T_u = 298 K, P_u = 1 bar, and φ = 0.9.

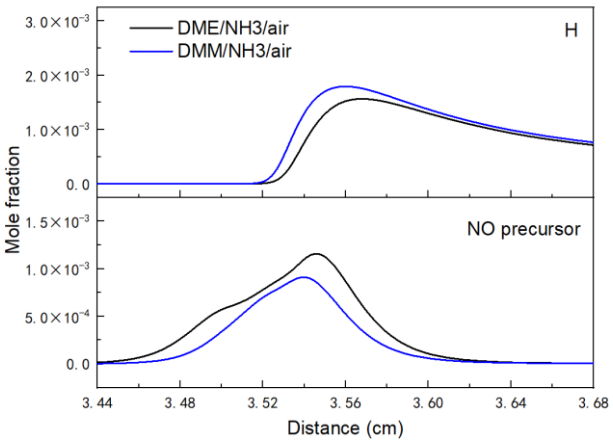

Figure 13. Concentration variations of the H radical and NO precursors under the conditions of T_u = 298 K, P_u = 1 bar, φ = 0.9, and X_{DME} = X_{DMM} = 40%.

4. Summary and Conclusions

In this study, we proposed a NH_3/DMM mechanism that can accurately predict the LBVs and IDTs of NH_3/DMM and NH_3/DME mixtures, which can be used as the

core mechanism for developing a combustion mechanism of NH_3 with heavier $PODE_n$. Furthermore, we conducted kinetic analysis of NH_3/DMM and NH_3/DME flames based on the present mechanism. Some of the key findings are as follows.

1. Updates of some key reactions using the latest dataset, e.g., NH, NNH, and H-relevant reactions and the interactions between DMM and NH_2/NO_x are crucial to increase the accuracy of the present mechanism.
2. Reaction path analysis revealed that early C–N interaction reactions play an important role in the oxidation pathway of NH_3. The dehydrogenation of NH_3 leads to the formation of NH_2, which then combines with a significant amount of CH_3 produced by the oxidation of DMM through collisions with other radicals, forming CH_3NH_2.
3. The analysis of NO_x emission shows that fuel NO_x coming from NH_3 dominates the NO_x emissions and NO turns out to be the main component of NO_x emissions.
4. The calculated NO_x emissions initially increase and then decrease with higher DME or DMM fraction, reaching a peak around a fraction of 40%. This phenomenon can be attributed to the 'trade-off' relationship between the high-activity radicals (e.g., H, OH, and O) and NO precursors promoted by the addition of DME or DMM.
5. The difference in NO_x mole fraction between NH_3/DMM and NH_3/DME flames does not exceed 830 ppm according to the calculations.

Supplementary Materials: The following supporting information can be downloaded at: https://www.mdpi.com/article/10.3390/en16196929/s1.

Author Contributions: Conceptualization, L.D. and C.Y.; validation, Y.Z. and M.Z.; formal analysis, Y.Z., C.Y. and Q.W.; writing—original draft preparation, Y.Z.; writing—review and editing, L.D. and C.Y.; supervision, L.D. and C.Y. All authors have read and agreed to the published version of the manuscript.

Funding: This research was funded by National Natural Science Foundation of China, grant number NO. 52206149.

Data Availability Statement: The mechanism developed in this study can be found in the Supplementary Material.

Acknowledgments: We acknowledge support by the KIT-Publication Fund of the Karlsruhe Institute of Technology.

Conflicts of Interest: The authors declare no conflict of interest.

Nomenclature

LBV	laminar burning velocity
IDT	ignition delay time
ROP	rate of production
NH_3	ammonia
NO_x	nitrogen oxides
DME	dimethyl ether
DMM	dimethoxymethane
$PODE_n$	polyoxymethylene dimethyl ethers
C_2	compounds containing two carbon atoms
C–N	carbon and nitrogen
T_u, T	temperature
P_u, P	pressure
V	reactor volume
c_v	heat capacity at constant volume
c_p	heat capacity at constant pressure
ρ	density

R	gas constant
X_{DME}	DME fraction
X_{DMM}	DMM fraction
$\dot{m}_{in}$	mass flow rates of reactants entering the reactor.
$\dot{m}_{out}$	mass flow rates of products leaving the reactor.
$\dot{q}$	heat sources or losses
u	axial velocity
Λ	pressure eigenvalue
μ	dynamic viscosity
λ	thermal conductivity
W_k	molecular weight of species *k*
Y_k	mole fraction of species *k*
$\dot{m}_k$	mass flow rates of each species
h_k	enthalpy of species *k*
$\dot{\omega}_k$	molar production rate of species *k*
j_k	diffusive mass flux of species *k*
φ	equivalence ratio
k_i	the rate constant of the *i*-th reaction
S_l	laminar burning velocity
S_i	normalized sensitivity coefficients

References

1. Chiong, M.C.; Chong, C.T.; Ng, J.H.; Mashruk, S.; Chong, W.W.F.; Samiran, N.A.; Mong, G.R.; Valera-Medina, A. Advancements of Combustion Technologies in the Ammonia-Fuelled Engines. *Energy Convers. Manag.* **2021**, *244*, 114460. [CrossRef]
2. Kang, L.; Pan, W.; Zhang, J.; Wang, W.; Tang, C. A Review on Ammonia Blends Combustion for Industrial Applications. *Fuel* **2023**, *332*, 126150. [CrossRef]
3. Verkamp, F.J.; Hardin, M.C.; Williams, J.R. Ammonia Combustion Properties and Performance in Gas-Turbine Burners. *Symp. Combust.* **1967**, *11*, 985–992. [CrossRef]
4. Starkman, E.S.; Samuelsen, G.S. Flame-Propagation Rates in Ammonia-Air Combustion at High Pressure. *Symp. Combust.* **1967**, *11*, 1037–1045. [CrossRef]
5. Wang, N.; Huang, S.; Zhang, Z.; Li, T.; Yi, P.; Wu, D.; Chen, G. Laminar Burning Characteristics of Ammonia/Hydrogen/Air Mixtures with Laser Ignition. *Int. J. Hydrogen Energy* **2021**, *46*, 31879–31893. [CrossRef]
6. Dai, L.; Gersen, S.; Glarborg, P.; Levinsky, H.; Mokhov, A. Experimental and Numerical Analysis of the Autoignition Behavior of NH_3 and NH_3/H_2 Mixtures at High Pressure. *Combust. Flame* **2020**, *215*, 134–144. [CrossRef]
7. Tian, Z.; Li, Y.; Zhang, L.; Glarborg, P.; Qi, F. An Experimental and Kinetic Modeling Study of Premixed $NH_3/CH_4/O_2/Ar$ Flames at Low Pressure. *Combust. Flame* **2009**, *156*, 1413–1426. [CrossRef]
8. Wang, D.; Wang, Z.; Zhang, T.; Zhai, Y.; Hou, R.; Tian, Z.Y.; Ji, C. A Comparative Study on the Laminar C1–C4 n-Alkane/NH_3 Premixed Flame. *Fuel* **2022**, *324*, 124732. [CrossRef]
9. Wang, Z.; Han, X.; He, Y.; Zhu, R.; Zhu, Y.; Zhou, Z.; Cen, K. Experimental and Kinetic Study on the Laminar Burning Velocities of NH_3 Mixing with CH3OH and C2H5OH in Premixed Flames. *Combust. Flame* **2021**, *229*, 111392. [CrossRef]
10. Xu, H.; Wang, J.; Zhang, C.; Dai, L.; He, Z.; Wang, Q. Numerical Study on Laminar Burning Velocity of Ammonia Flame with Methanol Addition. *Int. J. Hydrogen Energy* **2022**, *47*, 28152–28164. [CrossRef]
11. Okafor, E.C.; Naito, Y.; Colson, S.; Ichikawa, A.; Kudo, T.; Hayakawa, A.; Kobayashi, H. Measurement and Modelling of the Laminar Burning Velocity of Methane-Ammonia-Air Flames at High Pressures Using a Reduced Reaction Mechanism. *Combust. Flame* **2019**, *204*, 162–175. [CrossRef]
12. Mei, B.; Zhang, X.; Ma, S.; Cui, M.; Guo, H.; Cao, Z.; Li, Y. Experimental and Kinetic Modeling Investigation on the Laminar Flame Propagation of Ammonia under Oxygen Enrichment and Elevated Pressure Conditions. *Combust. Flame* **2019**, *210*, 236–246. [CrossRef]
13. Shrestha, K.P.; Lhuillier, C.; Barbosa, A.A.; Brequigny, P.; Contino, F.; Mounaïm-Rousselle, C.; Seidel, L.; Mauss, F. An Experimental and Modeling Study of Ammonia with Enriched Oxygen Content and Ammonia/Hydrogen Laminar Flame Speed at Elevated Pressure and Temperature. *Proc. Combust. Inst.* **2021**, *38*, 2163–2174. [CrossRef]
14. Glarborg, P.; Miller, J.A.; Ruscic, B.; Klippenstein, S.J. Modeling Nitrogen Chemistry in Combustion. *Prog. Energy Combust. Sci.* **2018**, *67*, 31–68. [CrossRef]
15. Klippenstein, S.J.; Harding, L.B.; Glarborg, P.; Miller, J.A. The Role of NNH in NO Formation and Control. *Combust. Flame* **2011**, *158*, 774–789. [CrossRef]
16. Mathieu, O.; Petersen, E.L. Experimental and Modeling Study on the High-Temperature Oxidation of Ammonia and Related NOx Chemistry. *Combust. Flame* **2015**, *162*, 554–570. [CrossRef]

17. Shrestha, K.P.; Seidel, L.; Zeuch, T.; Mauss, F.; Chemie, P.; Göttingen, G.; Gmbh, L.D.; Chaussee, B. Combustion A Detailed Kinetic Mechanism for the Oxidation of Ammonia Including the Formation and Reduction of Nitrogen Oxides. *Energy Fuels* **2018**, *32*, 10202–10217. [CrossRef]
18. Wang, B.; Dong, S.; Jiang, Z.; Gao, W.; Wang, Z.; Li, J.; Yang, C.; Wang, Z.; Cheng, X. Development of a Reduced Chemical Mechanism for Ammonia/n-Heptane Blends. *Fuel* **2023**, *338*, 127358. [CrossRef]
19. Chang, Y.; Jia, M.; Wang, P.; Niu, B.; Liu, J. Construction and Derivation of a Series of Skeletal Chemical Mechanisms for N-Alkanes with Uniform and Decoupling Structure Based on Reaction Rate Rules. *Combust. Flame* **2022**, *236*, 111785. [CrossRef]
20. Dong, S.; Wang, B.; Jiang, Z.; Li, Y.; Gao, W.; Wang, Z.; Cheng, X.; Curran, H.J. An Experimental and Kinetic Modeling Study of Ammonia/n -Heptane Blends. *Combust. Flame* **2022**, *246*, 112428. [CrossRef]
21. Pellegrini, L.; Marchionna, M.; Patrini, R.; Beatrice, C.; Del Giacomo, N.; Guido, C. Combustion Behaviour and Emission Performance of Neat and Blended Polyoxymethylene Dimethyl Ethers in a Light-Duty Diesel Engine. *SAE Tech. Pap.* **2012**, *01*, 1053. [CrossRef]
22. Li, B.; Li, Y.; Liu, H.; Liu, F.; Wang, Z.; Wang, J. Combustion and Emission Characteristics of Diesel Engine Fueled with Biodiesel/PODE Blends. *Appl. Energy* **2017**, *206*, 425–431. [CrossRef]
23. Yin, G.; Li, J.; Zhou, M.; Li, J.; Wang, C.; Hu, E.; Huang, Z. Experimental and Kinetic Study on Laminar Flame Speeds of Ammonia/Dimethyl Ether/Air under High Temperature and Elevated Pressure. *Combust. Flame* **2022**, *238*, 111915. [CrossRef]
24. Xiao, H.; Li, H. Experimental and Kinetic Modeling Study of the Laminar Burning Velocity of NH_3/DME/Air Premixed Flames. *Combust. Flame* **2022**, *245*, 16–19. [CrossRef]
25. Dai, L.; Hashemi, H.; Glarborg, P.; Gersen, S.; Marshall, P.; Mokhov, A.; Levinsky, H. Ignition Delay Times of NH_3/DME Blends at High Pressure and Low DME Fraction: RCM Experiments and Simulations. *Combust. Flame* **2021**, *227*, 120–134. [CrossRef]
26. Issayev, G.; Giri, B.R.; Elbaz, A.M.; Shrestha, K.P.; Mauss, F.; Roberts, W.L.; Farooq, A. Ignition Delay Time and Laminar Flame Speed Measurements of Ammonia Blended with Dimethyl Ether: A Promising Low Carbon Fuel Blend. *Renew. Energy* **2022**, *181*, 1353–1370. [CrossRef]
27. Zhao, Z.; Chaso, M.; Kazakov, A. Thermal Decomposition Reaction and a Comprehensive Kinetic Model of Dimethyl Ether. *Int. J. Chem. Kinet.* **2007**, *43*, 154–160. [CrossRef]
28. Han, X.; Wang, Z.; He, Y.; Zhu, Y.; Cen, K. Experimental and Kinetic Modeling Study of Laminar Burning Velocities of NH_3/Syngas/Air Premixed Flames. *Combust. Flame* **2020**, *213*, 1–13. [CrossRef]
29. Shrestha, K.P.; Eckart, S.; Elbaz, A.M.; Giri, B.R.; Fritsche, C.; Seidel, L.; Roberts, W.L.; Krause, H.; Mauss, F. A Comprehensive Kinetic Model for Dimethyl Ether and Dimethoxymethane Oxidation and NOx Interaction Utilizing Experimental Laminar Flame Speed Measurements at Elevated Pressure and Temperature. *Combust. Flame* **2020**, *218*, 57–74. [CrossRef]
30. Capriolo, G.; Brackmann, C.; Lubrano Lavadera, M.; Methling, T.; Konnov, A.A. An Experimental and Kinetic Modeling Study on Nitric Oxide Formation in Premixed C3alcohols Flames. *Proc. Combust. Inst.* **2021**, *38*, 805–812. [CrossRef]
31. Meng, X.; Zhang, M.; Zhao, C.; Tian, H.; Tian, J.; Long, W.; Bi, M. Study of Combustion and NO Chemical Reaction Mechanism in Ammonia Blended with DME. *Fuel* **2022**, *319*, 123832. [CrossRef]
32. Gross, C.W.; Kong, S.C. Performance Characteristics of a Compression-Ignition Engine Using Direct-Injection Ammonia-DME Mixtures. *Fuel* **2013**, *103*, 1069–1079. [CrossRef]
33. Elbaz, A.M.; Giri, B.R.; Issayev, G.; Shrestha, K.P.; Mauss, F.; Farooq, A.; Roberts, W.L. Experimental and Kinetic Modeling Study of Laminar Flame Speed of Dimethoxymethane and Ammonia Blends. *Energy Fuels* **2020**, *34*, 14726–14740. [CrossRef]
34. Shrestha, K.P.; Vin, N.; Herbinet, O.; Seidel, L.; Battin-Leclerc, F.; Zeuch, T.; Mauss, F. Insights into Nitromethane Combustion from Detailed Kinetic Modeling—Pyrolysis Experiments in Jet-Stirred and Flow Reactors. *Fuel* **2020**, *261*, 116349. [CrossRef]
35. Sun, W.; Wang, G.; Li, S.; Zhang, R.; Yang, B.; Yang, J.; Li, Y.; Westbrook, C.K.; Law, C.K. Speciation and the Laminar Burning Velocities of Poly(Oxymethylene) Dimethyl Ether 3 (POMDME3) Flames: An Experimental and Modeling Study. *Proc. Combust. Inst.* **2017**, *36*, 1269–1278. [CrossRef]
36. Li, N.; Sun, W.; Liu, S.; Qin, X.; Zhao, Y.; Wei, Y.; Zhang, Y. A Comprehensive Experimental and Kinetic Modeling Study of Dimethoxymethane Combustion. *Combust. Flame* **2021**, *233*, 111583. [CrossRef]
37. Goodwin, D.G.; Moffat, H.K.; Schoegl, I.; Speth, R.L.; Weber, B.W. Cantera: An object-oriented software toolkit for chemical kinetics, thermodynamics, and transport processes (Version 2.4.0). Available online: http://www.cantera.org (accessed on 16 October 2022).
38. Felden, A. *Cantera Tutorials—A Series of Tutorials to Get Started with the Python Interface of Cantera*, 1st ed.; Cerfacs: Toulouse, France, 2015; pp. 37–87.
39. Curran, H.J.; Gaffuri, P.; Pitz, W.J.; Westbrook, C.K. A Comprehensive Modeling Study of n-Heptane Oxidation. *Combust. Flame* **1998**, *114*, 149–177. [CrossRef]
40. Wang, Z.; Ji, C.; Wang, D.; Zhang, T.; Zhai, Y.; Wang, S. Experimental and Numerical Study on Laminar Burning Velocity and Premixed Combustion Characteristics of NH_3/C_3H_8/Air Mixtures. *Fuel* **2023**, *331*, 125936. [CrossRef]
41. Li, Y.; Sarathy, S.M. Probing Hydrogen–Nitrogen Chemistry: A Theoretical Study of Important Reactions in NxHy, HCN and HNCO Oxidation. *Int. J. Hydrogen Energy* **2020**, *45*, 23624–23637. [CrossRef]
42. Nakamura, H.; Hasegawa, S.; Tezuka, T. Kinetic Modeling of Ammonia/Air Weak Flames in a Micro Flow Reactor with a Controlled Temperature Profile. *Combust. Flame* **2017**, *185*, 16–27. [CrossRef]

43. Fernandes, R.X.; Luther, K.; Troe, J.; Ushakov, V.G. Experimental and Modelling Study of the Recombination Reaction H + O_2 (+M) → HO_2 (+M) between 300 and 900 K, 1.5 and 950 Bar, and in the Bath Gases M = He, Ar, and N_2. *Phys. Chem. Chem. Phys.* **2008**, *10*, 4313–4321. [CrossRef] [PubMed]
44. GRI-Mech 3.0—University of California, Berkeley. Available online: http://combustion.berkeley.edu/gri-mech/version30/text30.html (accessed on 12 March 2023).
45. Sutherland, J.W.; Patterson, P.M.; Klemm, R.B. Rate Constants for the Reaction, O(3P)+H_2O=OH+OH, over the Temperature Range 1053 K to 2033 K Using Two Direct Techniques. *Symp. Combust.* **1990**, *23*, 51–57. [CrossRef]
46. Burke, M.P.; Goldsmith, C.F.; Klippenstein, S.J.; Welz, O.; Huang, H.; Antonov, I.O.; Savee, J.D.; Osborn, D.L.; Zádor, J.; Taatjes, C.A.; et al. Multiscale Informatics for Low-Temperature Propane Oxidation: Further Complexities in Studies of Complex Reactions. *J. Phys. Chem. A* **2015**, *119*, 7095–7115. [CrossRef]
47. Baulch, H.M.; Schindler, D.W.; Turner, M.A.; Findlay, D.L.; Paterson, M.J.; Vinebrooke, R.D. Effects of Warming on Benthic Communities in a Boreal Lake: Implications of Climate Change. *Limnol. Oceanogr.* **2005**, *50*, 1377–1392. [CrossRef]
48. Joshi, A.V.; Wang, H. Master Equation Modeling of Wide Range Temperature and Pressure Dependence of CO + OH → Products. *Int. J. Chem. Kinet.* **2006**, *38*, 57–73. [CrossRef]
49. Vermeire, F.H.; Carstensen, H.H.; Herbinet, O.; Battin-Leclerc, F.; Marin, G.B.; Van Geem, K.M. Experimental and Modeling Study of the Pyrolysis and Combustion of Dimethoxymethane. *Combust. Flame* **2018**, *190*, 270–283. [CrossRef]
50. Jacobs, S.; Döntgen, M.; Alquaity, A.B.S.; Kopp, W.A.; Kröger, L.C.; Burke, U.; Pitsch, H.; Leonhard, K.; Curran, H.J.; Heufer, K.A. Detailed Kinetic Modeling of Dimethoxymethane. Part II: Experimental and Theoretical Study of the Kinetics and Reaction Mechanism. *Combust. Flame* **2019**, *205*, 522–533. [CrossRef]
51. Lhuillier, C.; Brequigny, P.; Lamoureux, N.; Contino, F.; Mounaïm-Rousselle, C. Experimental Investigation on Laminar Burning Velocities of Ammonia/Hydrogen/Air Mixtures at Elevated Temperatures. *Fuel* **2020**, *263*, 116653. [CrossRef]
52. Han, X.; Wang, Z.; Costa, M.; Sun, Z.; He, Y.; Cen, K. Experimental and Kinetic Modeling Study of Laminar Burning Velocities of NH_3/Air, NH_3/H_2/Air, NH_3/CO/Air and NH_3/CH_4/Air Premixed Flames. *Combust. Flame* **2019**, *206*, 214–226. [CrossRef]
53. Li, R.; Konnov, A.A.; He, G.; Qin, F.; Zhang, D. Chemical Mechanism Development and Reduction for Combustion of NH_3/H_2/CH_4 Mixtures. *Fuel* **2019**, *257*, 116059. [CrossRef]